NEOPLASIA
www.neoplasia.com

Volume 12 Number 2 February 2010 pp. 150–160 150

Translocation of p53 to Mitochondria Is Regulated by Its Lipid Binding Property to Anionic Phospholipids and It Participates in Cell Death Control[1]

Ching-Hao Li*, Yu-Wen Cheng†, Po-Ling Liao* and Jaw-Jou Kang*

*Institute of Toxicology, College of Medicine, National Taiwan University, Taipei, Taiwan; †School of Pharmacy, Taipei Medicine University, Taipei, Taiwan

Abstract

p53, can regulate cell apoptosis in both transcription-dependent and -independent manners. The transcription-independent pathway was demonstrated by the translocation of p53 to mitochondria. Our study showed that p53 mitochondrial translocation was found in mitomycin C (MMC)–treated HepG2. The p53 C-terminal domain is clustered with potential nuclear leading sequences and showed strong electrostatic ion-ion interactions with cardiolipin, phosphatidylglycerol and phosphatidic acid *in vitro*. Disruption of cardiolipin biosynthesis by phosphatidylglycerophosphate synthase (PGS) or CDP-diacylglycerol synthase 2 (CDS-2) short hairpin RNA (shRNA) transfection eliminated the MMC-induced translocation of mitochondrial p53. The elimination of mitochondrial p53 translocation also reduced Bcl-xL and Bcl-2 mitochondrial distribution. In HEK 293T models with saturated p53 expression, the mitochondrial partition of p53, Bcl-xL, and Bcl-2 obviously decreased in their PGS shRNA- or CDS-2 shRNA-expressing stable clones. In p53-null H1299 models, both the mitochondrial partitions of Bcl-xL and Bcl-2 were strongly reduced in relation to the HEK 293T models. The Bcl-xL mitochondrial partition was elevated in H1299 models expressing pCEP4-p53wt suggesting the direct carrier role of p53 in transporting Bcl-xL to the mitochondria. We also found that the cytosolic pool of Bcl-xL and Bcl-2 remained unaffected in the low-dose MMC treatment but decreased in the high-dose MMC treatment. The cytosolic pool of Bcl-2 and Bcl-xL directly regulated their amounts in p53-dependent mitochondrial distribution. In the low-dose MMC treatment, the increased mitochondrial p53, Bcl-xL, and Bcl-2 could attenuate apoptosis. However, in the high-dose MMC treatment, only the p53 translocated to the mitochondria and resulted in apoptosis progression. On the basis of this study, we thought mitochondrial p53 might regulate apoptosis in a biphasic manner.

Neoplasia (2010) 12, 150–160

Introduction

p53 was the first tumor suppressor gene identified in 1979. The p53 protein consists of 393 amino acids, and its structure is subdivided into an N-terminal transactivation domain, a central DNA-binding domain, and a C-terminal domain [1–3]. Once activated, p53 is phosphorylated and it escapes from ubiquitin degradation. Activated p53 shows multiple functions including cell cycle regulation [2], DNA repair, and apoptosis [4–7]. p53-Associated apoptotic regulation can be achieved in a transcription-dependent or -independent manner. p53-Dependent transcription of mitochondria-anchored proapoptotic products [5,6] and p53-inducible genes [4,7] disrupts mitochondrial integrity and causes cytochrome *c* release. The transcription-independent apoptotic signal is induced by p53 protein-protein interactions in the mitochondria

Abbreviations: 293T-PGS shRNA, PGS shRNA-transfected 293T cell; CDS-2, CDP-diacylglycerol synthase 2; CLS, cardiolipin synthase; Cox I, cytochrome *c* oxidase subunit I; HepG2-PGS shRNA, PGS shRNA-transfected HepG2 cell; MMC, mitomycin C; NLS, nuclear leading sequence; PGS, phosphatidylglycerophosphate synthase; shRNA, short hairpin RNA

Address all correspondence to: Jaw-Jou Kang, PhD, Institute of Toxicology, College of Medicine, National Taiwan University, No, 1 Jen-Ai Rd, Section 1, Taipei, Taiwan.
E-mail: jjkang@ntu.edu.tw

[1]This article refers to supplementary materials, which are designated by Figures W1 to W3 and are available online at www.neoplasia.com.

Received 2 September 2009; Revised 19 November 2009; Accepted 23 November 2009

DOI 10.1593/neo.91500

[8,9]. Candidate proteins interacting with p53 in the mitochondria were identified one by one [10–14]. However, the mechanism by which p53 is translocated to mitochondria is still unknown.

Cardiolipin (1,3-bis (19,29-diacyl-39-phosphoryl-*sn*-glycerol)-*sn*-glycerol) is a mitochondria-restricted, anionic, asymmetric phospholipid. Cardiolipin is the major component of mitochondria phospholipids (comprising approximately 8%-15%) of both the outer and the inner membranes [15,16]. Cardiolipin biosynthesis is regulated by the CDP-diacylglycerol synthase (CDS) that converts phosphatidic acid to CDP-diacylglycerol. Phosphatidylglycerophosphate synthase (PGS, EC 2.7.8.5) catalyzes the formation of phosphatidylglycerophosphate from CDP-diacylglycerol and glycerol-3-phosphate. Phosphatidylglycerophosphate is then dephosphorylated to phosphatidylglycerol by phosphatidylglycerophosphate phosphatase. Then, cardiolipin synthase (CLS) converts phosphatidylglycerol to cardiolipin through condensation with CDP-diacylglycerol [15–17]. Human CLS was identified and cloned in 2006 [18]. The functional mutation of PGS and CLS was demonstrated to cause cardiolipin depletion. Cardiolipin-depleted cells often show electron transport inhibition [19], changes in ion permeability and membrane integrity [19], a decrease in protein importation [20], and collapse of mitochondria membrane potential [20,21]. These findings suggest the crucial physiological and pathological position of cardiolipin in the mitochondria.

In the present study, the mitochondrial translocation of p53 was investigated in mitomycin C (MMC)–treated cells. We found that cardiolipin tightly bound to the C-terminal region of p53 protein *in vitro*. Down-regulation of PGS and CDS protein expressions diminished the content of p53 translocation to the mitochondria, suggesting that a specific p53-cardiolipin interaction is an important step in triggering its mitochondrial distribution. Moreover, the p53 protein was also demonstrated to interact with Bcl-xL [10,11], and the p53–Bcl-xL protein interaction might lead to Bcl-xL mitochondrial translocation and cell death regulation.

Materials and Methods

Cell Culture

The hepatocarcinoma cell line HepG2, the adenocarcinoma cell line A549, the HEK 293T cells with endogenous wild-type p53, and the p53-null H1299 cells were purchased from American Type Culture Collection (ATCC; Manassas, VA). All cell lines were maintained in Dulbecco's modified Eagle medium with 10% heat-inactivated fetal bovine serum in a humidified atmosphere of 5% CO_2 in a 37°C incubator. The CDP-diacylglycerol synthase 2 (CDS-2) short hairpin RNA (shRNA)- and PGS shRNA-expressing stable clones were selected from transfected HEK 293T and H1299 cells, respectively, by the addition of 1 μg/ml puromycin.

Transfection

Transfection was performed by using PolyJet *in vitro* DNA transfection reagent (SignaGen Laboratory, Gaithersburg, MD) at 24 hours after seeding. CDP-diacylglycerol synthase-2 (CDS-2, TRCN0000035859) and PGS (TRCN0000045342) shRNA pLKO.1-puro constructs were purchased from the National RNAi Core Facility (Academia Sinica, Taipei, Taiwan). The pCEP4 vector and pCEP4-p53wt were kindly provided by Dr. Tzeng SL (Chung Shan Medical University). Briefly, 1 to 5 μg of shRNA or plasmid and PolyJet reagent were respectively diluted within an incomplete Dulbecco's modified Eagle medium, then mixed vigorously and incubated at room temperature. Twenty minutes later, the mixture was layered on serum-free culture medium. Cells were transfected for at least 6 hours.

Isolation and Purification of Mitochondria

Treated cells were incubated in hypotonic buffer for 10 minutes, followed by a homogenizing procedure for 10 seconds, five to six times. The cell debris was separated by the first centrifugation at 1200*g* for 10 minutes. The supernatant was transferred to tubes, and the heavy membrane pellet enriched in the mitochondria was isolated by the second centrifugation at 10,000*g* for 10 minutes. The mitochondria-enriched fraction was layered on a discontinuous sucrose gradient (1.0 M and 1.5 M sucrose prepared in 5 mM EDTA, 10 mM Tris-HCl, pH 7.4). Finally, mitochondria were purified from the 1.0/1.5 M interface after a third centrifugation.

Alkali Extraction

For alkali extraction [22], pure mitochondria were incubated with 100 mM Na_2CO_3 (pH 11.5) for 10 minutes on ice. The pellet separated by centrifugation at 12,000*g* was used as the integral membrane fraction. The supernatant was denoted the soluble fraction.

Western Blot Analysis

Intact cell lysates and mitochondria lysates were prepared using RIPA buffer (50 mM Tris-HCl (pH 7.4), 150 mM NaCl, 1 mM EGTA, 1 mM NaF, 1 mM Na_3VO_4, and proteinase inhibitor cocktail) containing 1% Nonidet P-40 or 1% dodecymaltoside, respectively. Protein concentration was determined by the Bradford method (Bio-Rad, CA). Adequate lysates were mixed well with sodium dodecylsulfate–polyacrylamide gel electrophoresis loading buffer and separated by 10% or 12% sodium dodecylsulfate–polyacrylamide gel electrophoresis. The separated proteins were electroblotted onto the polyvinylidene difluoride (PVDF) sheets. For immunodetection, the PVDF membrane was blocked in nonfat milk and incubated in Tris-buffered saline with Tween-20 with antibodies specific to p53 (05-224; Upstate Biotech, Lake Placid, NY), Mdm-2 (clone SMP14; NeoMarker, Fremont, CA), proliferating cell nuclear antigen (clone PC10; NeoMarker), Bax (clone 2D2; NeoMarker), Core II (A11143; Molecular Probes, Carlsbad, CA), PGS (H00009489; Abnova, Taipei, Taiwan), CDS-2 (H00008760; Abnova), Bcl-2 (sc-509; Santa Cruz Biotechnology, Santa Cruz, CA), Bcl-xL (clone 2H12; eBiosciences, San Diego, CA), and β-actin (Sigma, Saint Louis, MO). For chemiluminescent detection, PVDF blots were incubated with horseradish peroxidase–conjugated secondary antibody (1:5000 in Tris-buffered saline with Tween-20) for 2 hours at room temperature, followed by enhanced chemiluminescence detection, according to the manufacturer's protocol (Millipore, Billerica, MA).

Confocal Microscopy

For immunofluorescent studies, cells were seeded on cover glasses. Treated cells were fixed and permeablized with ice-cold MeOH. The first antibodies' reactions specific to p53 (sc-6243; Santa Cruz Biotechnology), Histone H1 (sc-8030; Santa Cruz Biotechnology), cytochrome *c* oxidase subunit I (Cox I, A-6403; Molecular Probes) were performed overnight at 4°C (1: 200 dilution in phosphate-buffered saline with Tween). Conjugation of the secondary antibodies with fluorescein isothiocyanate or tetramethyl rhodamine isothiocyanate reaction (Santa Cruz Biotechnology) was performed at 25°C for 2 hours. Cells were observed under a Leica confocal laser microscope (Leica Microsystems, Wetzler, Germany) with excitation and emission at 488 and 543 nm, respectively.

Recombinant Fusion Protein Expression

pGEX-1 plasmids encoded with the sequences of full-length human p53, or p53 deletions or mutants, were transformed into *Escherichia coli* BL21 using calcium chloride. Recombinant fusion protein expression was performed by 0.25 mM isopropyl β-D-1-thiogalactopyranoside induction for 3 hours at 30°C [23]. Cells were lysed by sonication in phosphate-buffered saline (PBS) containing 1 mM dithiothreitol, 1 mM phenylmethylsulphonyl fluoride, 0.2 mM EDTA. After centrifugation, the glutathione S-transferase fusion protein in the supernatant was bound with 50% (vol./vol.) glutathione-agarose beads. The fusion protein was eluted by 50 mM Tris buffer (pH 7.5) with 50 mM reduced glutathione.

Lipid-Binding Assay

The interaction of recombinant p53 fusion protein and phospholipids was evaluated *in vitro* [22]. Fifty microliters per well of phospholipids (100 μg/ml dissolved in EtOH) was coated onto 96-well plates by evaporation at room temperature. The coated plates were tested within 24 hours. Target proteins diluted in phosphate-buffered saline with Tween (1-10 μg/ml) were incubated within microwells at 25°C for 2 hours. The specific protein-lipid interaction was detected by immunocolorimetric optical density of 3,3′,5,5′-tetramethylbenzidine at 450 nm.

Apoptotic Index Analysis

Cells seeded in six-well plates were treated as indicated. To identify and quantify DNA content, cells were trypsinized, fixed overnight in 70% ethanol, and then resuspended in PBS containing RNase A (10 μg/ml) and propidium iodide (25 μg/ml). Apoptotic cells with the sub-G_1 peak localized below the G_0/G_1 peak were identified by flow cytometry with FL2 filter [24].

Statistical Analysis

All data were expressed as mean ± SEM from at least three independent experiments. Statistical analysis was carried out by analysis of variance (SPSS 12.0, Sinter Information Group, Taipei, Taiwan), and $P < .05$ was considered significantly different.

Results

The Activated p53 Protein Was Found in Both Nuclear and Mitochondrial Fractions

The DNA damage agent MMC can induce endogenous p53 protein accumulation in both dose- and time-dependent manners in HepG2 cells. Interestingly, the activated p53 protein was also found in the purified mitochondria fraction (Figure 1, *A* and *B*). The mitochondrial marker, Core II, and the nuclear protein, proliferating cell nuclear antigen, were used for quality control of mitochondria fractionation (Figure 1*A*). MMC (5-10 μg/ml) treatment for 6 hours caused six- to eight-fold increases in mitochondrial p53 translocation (Figure 1*A*). In the time-dependent studies, 5 μg/ml MMC incubation for 3, 6, and 12 hours caused 4.8-, 6.7-, and 12.7-fold increases in mitochondrial p53 translocation (Figure 1*B*). The translocation of p53 protein to mitochondria was also observed by immunofluorescent staining. In intact A549 cells, the colocalization of p53 with nuclear histone H1 or mitochondria Cox I is shown in merged images (Figure 1*C*). Mitochondrial p53 translocation was also observed in p53-overexpressing H1299 cells (data not shown).

Mitochondrial p53 Was Displayed in Both the Membrane-Bound Form and Free Soluble Form

Unlike the membrane-integral Cox I protein, the mitochondrial p53 could be fully extracted by 100 mM alkali Na_2CO_3 (pH 11.5), suggesting that mitochondrial p53 retained its soluble characteristic (Figure 2*A*). However, in 1% dodecymaltoside detergent extraction, mitochondrial p53 was more resistant than the Cox I protein and was detected in both the soluble supernatant fraction (soluble form p53) and the insoluble pellet fraction (membrane-bound p53; Figure 2*B*).

Interaction of p53 with Cardiolipin through Its C-terminal Domain

The p53 protein-phospholipid interaction was evaluated by an *in vitro* lipid-binding assay [22]. The recombinant p53-GST fusion protein showed high lipid-binding properties with phosphatidylserine, phosphatidylglycerol, cardiolipin, and phosphatidic acid but showed lower lipid-binding properties to phosphatidylcholine, phosphatidylethanolamine, phosphatidylinositol, cholesterol, and sphingomyelin (Figure 2*C*). Both phosphatidic acid and phosphatidylglycerol were anionic and were precursors in cardiolipin biosynthesis [15–17]. The specific protein-lipid interactions were not found for GST protein itself (Figure 2*D*).

Subsequently, the cardiolipin-binding activities of recombinant mutant p53 protein (R175H), the N-terminal transactivation domain (p53-1~100), the DNA binding domain (p53-1~318 and p53-100~318) and the C-terminal domain (p53-319~393) were tested. The p53 C-terminal domain and R175H mutant showed strong cardiolipin-binding activities. The p53 fragments containing 100 to 318 polypeptides showed mild cardiolipin-binding activity. However, the N-terminal domain was irrelevant to p53-cardiolipin interaction (Figure 2*D*).

To determine if cardiolipin and cardiolipin precursors function as a carrier that transports p53 to the mitochondria, two key enzymes, PGS and CDS, that are implicated in cardiolipin biosynthesis were studied. Two CDS isoforms were identified in humans. CDS-1 is expressed in the retina and is implicated in phototransduction. CDS-2 has a widespread tissue distribution [25]. Therefore, CDS-2 was selected for further studies.

Down-regulation of PGS Expression Decreased Cellular p53 Translocation to the Mitochondria

The efficacy of PGS shRNA constructs was screened by dose-dependent transient transfection. The PGS shRNA construct (5 μg of plasmids/6-cm transfection) caused 90% suppression of PGS protein expression (Figure 3*A*) and decreased in cellular cardiolipin level (Figure W1). In the whole lysate analysis, MMC induced p53 and PGS expression in nontransfected control, vector control, and PGS shRNA-transfected HepG2 cells (HepG2-PGS shRNA). MMC-induced PGS expression might overwhelm the RNA interfering effect of the shRNA construct. Contents of the p53 translocation to the mitochondrial fraction showed no significant differences among nontransfected control, vector control, and HepG2-PGS shRNA (Figure 3*B*).

To resolve the RNA interfering problem, the p53 transactivation inhibitor, pifithrin-α (20 μM), was used for pretreatment and coincubation with MMC. Pifithrin-α inhibited transactivation of p53-responsive gene expression, including Mdm-2 and PGS, but was irrelevant to p53 accumulation in whole lysate (Figure 3*C*) and p53 mitochondrial translocation (Figure 3*D*). Therefore, in the very condition, pifithrin-α pretreatment is necessary to work against the PGS expression induced

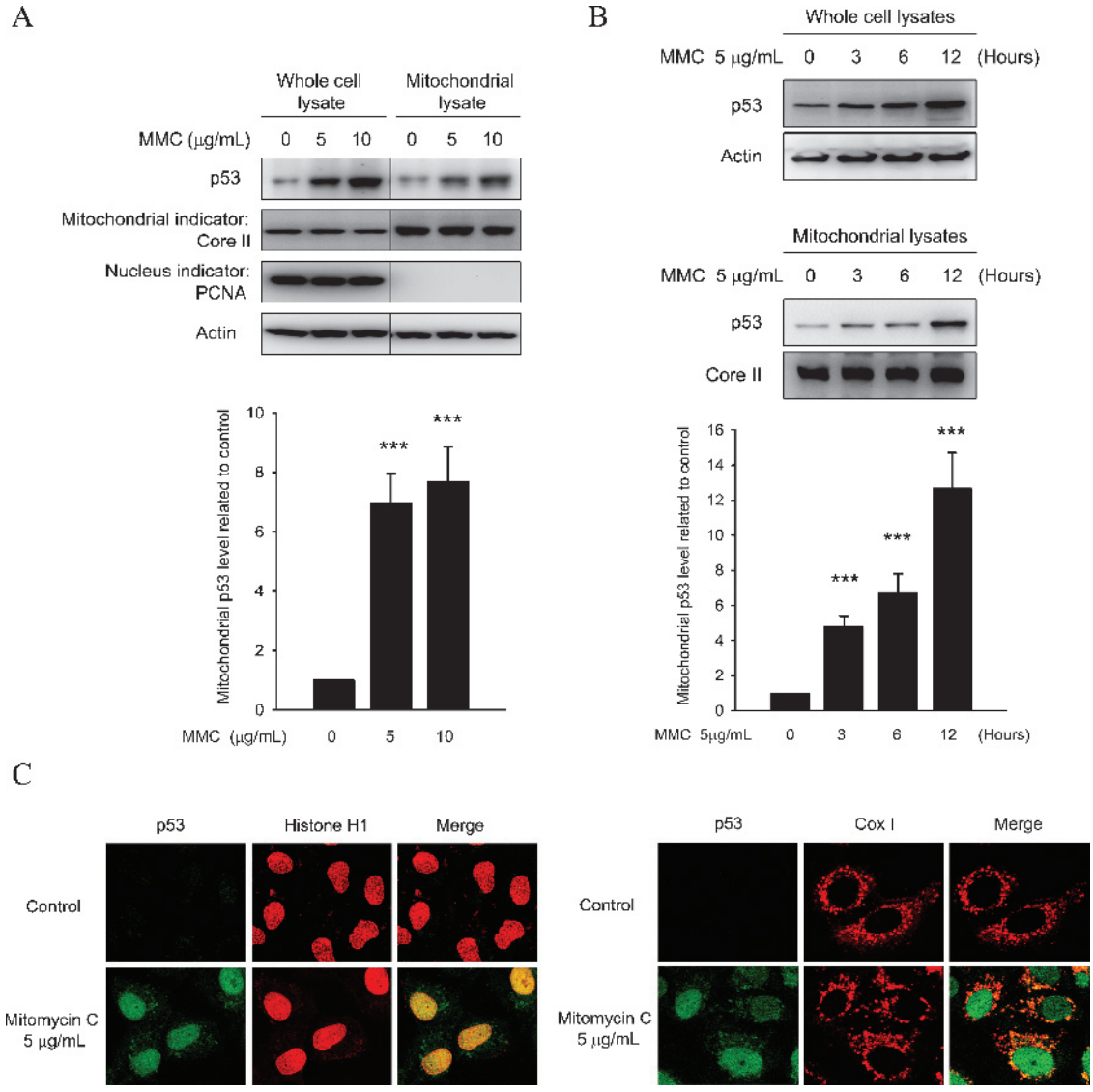

Figure 1. Activated p53 protein was found in both nuclear and mitochondrial fractions. Western blots showed that MMC treatments induced p53 accumulation in HepG2 whole-cell lysate and mitochondrial lysate in both dose-dependent (A) and time-dependent manners (B). In dose-dependent studies, 5 and 10 μg/ml MMC was treated for 6 hours. In the time-dependent studies, 5 μg/ml MMC was treated for 3, 6, and 12 hours. The core II protein was used as a mitochondrial internal control. The nuclear PCNA protein was used to identify the fractionation quality. The contents of mitochondrial p53 translocation were analyzed by densitometry. *$P < .05$, **$P < .01$, and ***$P < .001$, indicate statistical significance. (C) Immunofluorescent images showed the endogenous p53 was colocalized with nuclear histone H1 (left panel) and mitochondrial Cox I (right panel) in intact A549 cells.

by MMC treatment and make sure the successful knockdown of PGS protein. In Figure 3*E*, the p53 mitochondrial translocation reduced in the MMC-treated HepG2-PGS shRNA cell with pifithrin-α pretreatment, but the reduction would not take place without the pifithrin-α pretreatment. Therefore, we concluded that the decrease in mitochondrial p53 resulted directly from PGS protein knockdown rather than pifithrin-α.

Down-regulation of CDS-2 Expression Decreased Cellular p53 Translocation to the Mitochondria

Dose-dependent transient transfection studies showed that the CDS-2 shRNA construct (5 μg of plasmids/6-cm transfection) caused 80% suppression of CDS-2 protein expression (Figure 4*A*) and decreased cellular cardiolipin level (Figure W1). In the whole lysate analysis, MMC induced p53 accumulation in nontransfected control, vector control, and HepG2–CDS-2 shRNA cells. The content of p53 translocated to the mitochondria decreased in HepG2–CDS-2 shRNA cells (Figure 4*B*). These results showed that disruption of cardiolipin biosynthesis diminished the content of mitochondrial p53 translocation, suggesting the critical role of cardiolipin in p53 translocation to the mitochondria.

Decreased Mitochondrial p53 Content Enhanced MMC-Induced Cell Death

The effects of mitochondrial p53 content on cell death were evaluated by the sub-G_1 DNA formation. Before MMC treatment, the cell viabilities (Figure 5*A*) and resting caspase 3 activities (data not shown) were without significant changes among HepG2–wild-type, HepG2-PGS shRNA, and HepG2-CDS shRNA cells. MMC (5-20 μg/ml) treatment increased the sub-G_1 DNA population in a dose-dependent manner. MMC-induced apoptotic index remained unaffected by pifithrin-α

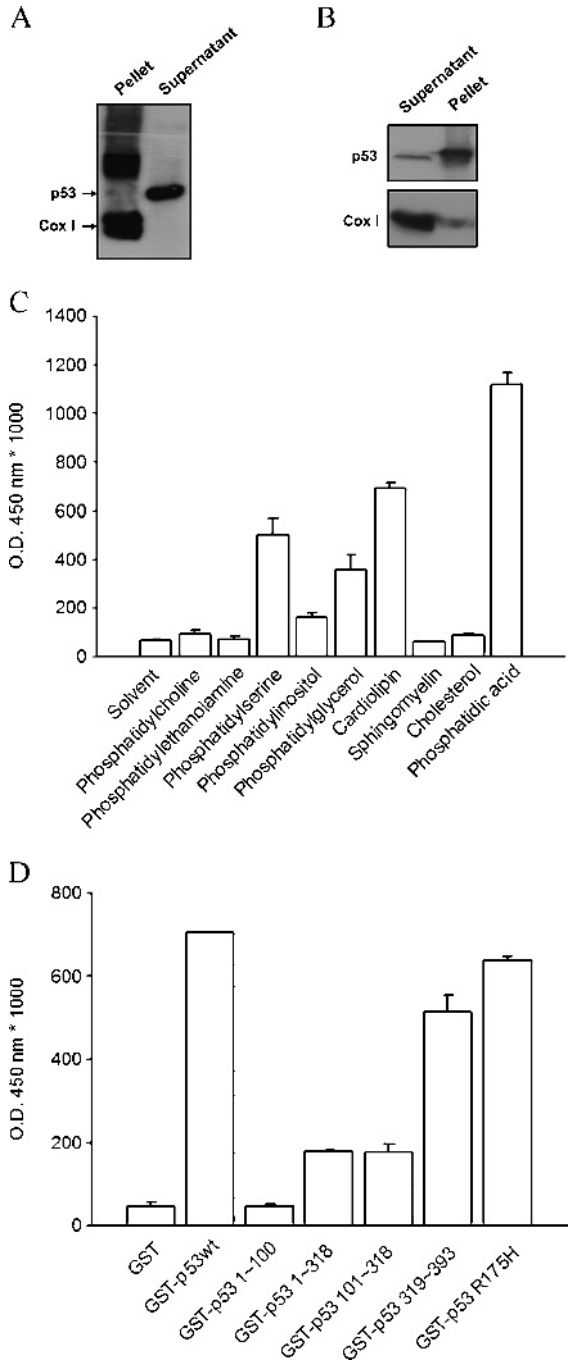

Figure 2. Determination of the characteristics of mitochondrial p53. (A) Alkali extraction showed that the mitochondrial p53 was detected in the supernatant fraction, suggesting that mitochondrial p53 retained its soluble characteristic. The membrane-integrated Cox I protein was detected in the pellet. (B) The 1% dodecymaltoside detergent extraction showed that mitochondrial p53 was more resistance than integrated Cox I protein, suggesting that both membrane-bound p53 (pellet) and free soluble form p53 (supernatant) coexisted in the mitochondria. (C) The association between p53 and phospholipids was evaluated by an *in vitro* lipid-binding assay. p53 displayed strong lipid-binding properties with anionic phospholipids including phosphatidylserine, cardiolipin, phosphatidylglycerol, and phosphatidic acid. (D) The p53 C-terminal domain and R175H mutant showed strong cardiolipin-binding activities. The p53 fragment containing 100 to 318 polypeptides showed mild cardiolipin-binding activity. The N-terminal domain was irrelevant to p53-cardiolipin interactions.

(20 μM) pretreatment (Figure 5*A*). In HepG2–CDS-2 shRNA and HepG2-PGS shRNA cells with pifithrin-α pretreatment, 5 to 10 μg/ml MMC treatments not only decreased mitochondrial p53 translocation content but also enhanced the apoptotic index, which showed an increase in sub-G_1 DNA fraction. However, in HepG2-PGS shRNA cell without pifithrin-α pretreatment, MMC-induced apoptotic indexes were without significant changes compared with MMC-treated HepG2–wild-type cell. In high-dose (20 μg/ml) MMC treatment, the apoptotic index was without statistical differences among HepG2–wild-type, HepG2-PGS shRNA, and HepG2-CDS shRNA cells (Figure 5*A*).

A Decrease in the p53-Dependent Bcl-xL and Bcl-2 Mitochondrial Distribution Facilitated Proapoptotic Status

The antiapoptotic Bcl-family members, Bcl-xL and Bcl-2, protein expression, and mitochondrial distribution were investigated. In Figure 5*B*, the MMC treatment was 5 μg/ml (low dose) and 20 μg/ml (high dose). In the 5 μg/ml MMC treatment for 6 hours, the Bcl-xL and Bcl-2 expression in whole lysate remained unaffected compared with control (Figure 5, *B* and *C*), whereas the increase in Bcl-xL and Bcl-2 mitochondrial distribution was found in their mitochondrial lysate (Figure 5, *B* and *D*). In HepG2–CDS-2 shRNA cells, as a limitation of mitochondrial p53 translocation, the mitochondrial distribution of Bcl-xL and Bcl-2 was diminished compared with HepG2–wild-type cell (Figure 5*D*), suggesting that the result was p53-dependent. But, in the 20 μg/ml MMC treatment, the Bcl-xL and Bcl-2 expression decreased obviously in the whole lysate (Figure 5, *B* and *C*). The decrease of Bcl-xL and Bcl-2 in cytosolic pool resulted in a reduction in their mitochondrial distribution, both in HepG2–wild-type and HepG2–CDS-2 shRNA cells (Figure 5*D*). The proapoptotic Bax protein expression was induced, which correlated with p53 accumulation, in both HepG2–wild-type and HepG2–CDS-2 shRNA whole cell lysates, and resulted in the increase of Bax protein in their mitochondrial fractions (Figure 5*B*). We thought the apoptotic enhancement in low-dose MMC-treated HepG2–CDS-2 shRNA cell might result from the limitation of mitochondrial p53 translocation and p53-dependent Bcl-xL and Bcl-2 mitochondrial distribution. But, in the high-dose MMC treatment, no apoptotic enhancement observed in HepG2–CDS-2 shRNA cell might result from the decrease in both Bcl-xL and Bcl-2 expression in cytosolic pool and in the p53-dependent Bcl-xL and Bcl-2 mitochondrial distribution.

p53 Protein Is a Crucial Factor in Bcl-xL and Bcl-2 Mitochondrial Distribution

To investigate the requirement of p53 for Bcl-xL and Bcl-2 mitochondrial distribution, stable clones of HEK 293T cells expressing PGS shRNA and CDS-2 shRNA were selected (Figure 6*A*). Wild-type 293T cells showed a higher basal level of cytosolic p53 protein compared with HepG2 cells. The addition of MMC did not increase cytosolic p53 protein accumulation in wild-type 293T and 293T stable clones, suggesting the saturation state of p53 content in their cytosol (Figure 6*B*). In 293T models, the mitochondrial p53 level was significantly reduced in 293T–CDS-2 shRNA and PGS shRNA-transfected 293T (293T-PGS shRNA) cells in relation to wild-type 293T (Figure 6*C*). In both 293T–CDS-2 shRNA and 293T-PGS shRNA cells, the Bcl-xL and Bcl-2 expressions were without significant changes in whole lysates, but the Bcl-xL and Bcl-2 mitochondrial distribution was obviously reduced (Figure 6, *C* and *D*). These results showed that disruption of cardiolipin biosynthesis in 293T models not only diminished

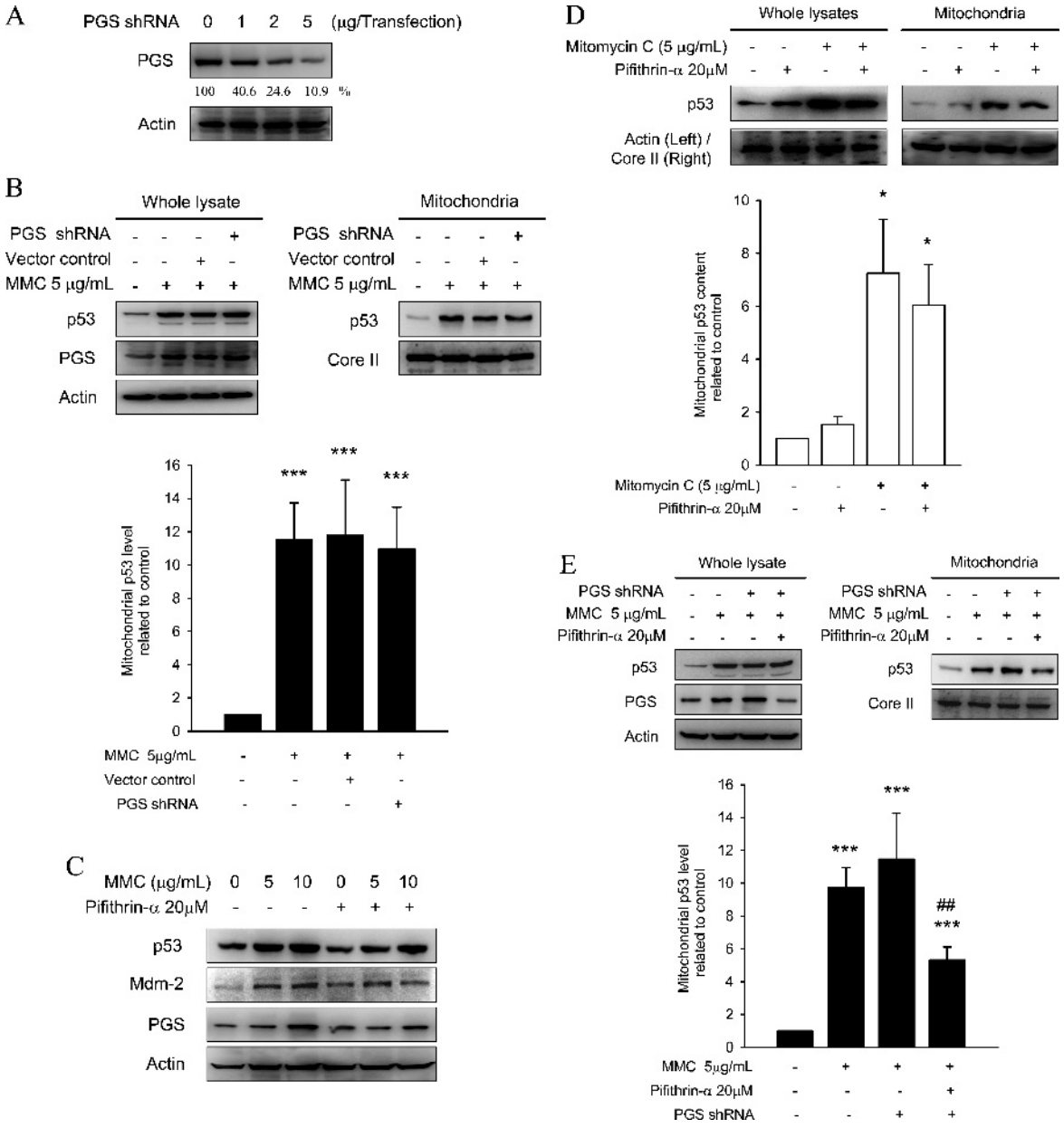

Figure 3. Down-regulation of PGS expression decreased cellular p53 translocation to mitochondria. (A) The PGS shRNA constructs (1-5 μg of plasmids/6-cm transfection) were transfected into the HepG2 cell for 24 hours as described in Materials and Methods. Western blots showed that PGS protein expression was downregulated. (B) Nontransfected control, vector control, and PGS shRNA-transfected cells were treated 5 μg/ml MMC for 12 hours, then total lysates were collected and analyzed by Western blots. The blots showed that both p53 and PGS were induced by MMC treatments. The mitochondria fraction was isolated as described in Materials and Methods. The contents of p53 translocated to the mitochondrial fraction showed no significant difference among nontransfected control, vector control, and PGS shRNA-transfected cells. The contents of mitochondrial p53 translocation were analyzed by densitometry. $^{*}P < .05$, $^{**}P < .01$, and $^{***}P < .001$, indicate a significant difference with the control. $^{\#}P < .05$, $^{\#\#}P < .01$, and $^{\#\#\#}P < .001$, indicate a significant difference with the MMC-treated control. (C) The p53 transactivation inhibitor, pifithrin-α (20 μM), was pretreated and coincubated with 5 to 10 μg/ml MMC for 24 hours. Pifithrin-α inhibited p53-responsive Mdm2 and PGS induction but was irrelevant to p53 accumulation. (D) To determine the effect of pifithrin-α treatment on p53 mitochondrial translocation, HepG2 was pretreated with pifithrin-α for 30 minutes, followed by MMC treatment for 12 hours. The blots showed that both p53 levels in whole and in mitochondrial lysates remained unaffected by pifithrin-α. (E) The nontransfected control and PGS shRNA-transfected cells with or without pifithrin-α (20 μM) pretreatment were treated 5 μg/ml MMC for 12 hours, then total lysates were collected and analyzed by Western blots. The blots showed that PGS expression was blocked in PGS shRNA-transfected cells with pifithrin-α pretreatments. The contents of p53 translocated to the mitochondrial fraction significantly decreased in PGS shRNA-transfected cells with pifithrin-α pretreatments. The contents of mitochondrial p53 translocation were analyzed by densitometry.

the content of mitochondrial p53 translocation but also reduced Bcl-xL and Bcl-2 translocation to the mitochondria.

To exclude the interferences form different expression levels of Bcl-xL and Bcl-2 among 293T models, the "Bcl-$2_{mitochondria/whole}$" and "Bcl-$xL_{mitochondria/whole}$" ratios were calculated. The higher ratio reflected the higher Bcl-xL and Bcl-2 partition to mitochondria rather than to the cytosolic fraction. The Bcl-$2_{mitochondria/whole}$ and Bcl-xL $_{mitochondria/whole}$ ratio significantly decreased in 293T–CDS-2 shRNA

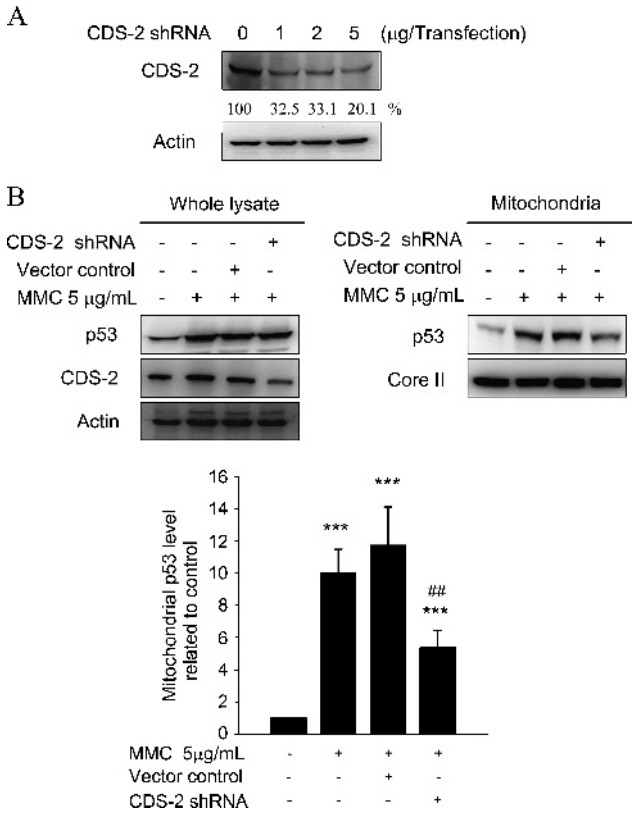

Figure 4. Down-regulation of CLS (CDS-2) expression decreased cellular p53 translocation to the mitochondria. (A) The CDS-2 shRNA constructs (1-5 μg of plasmids/6-cm transfection) were transfected into HepG2 cell for 24 hours as described in Materials and Methods. Western blots showed that the CDS-2 protein expression was down-regulated. (B) Nontransfected control, vector control, and CDS-2 shRNA-transfected cells were treated 5 μg/ml MMC for 12 hours, then total lysates were collected and analyzed by Western blots. The blots showed p53 was induced by MMC treatments. After 5 μg/ml MMC treatment for 12 hours, the mitochondria fraction was isolated as described in Materials and Methods. The contents of p53 translocation to the mitochondrial fraction significantly decreased in CDS-2 shRNA-transfected cells. The contents of mitochondrial p53 translocation were analyzed by densitometry. $^{*}P < .05$, $^{**}P < .01$, and $^{***}P < .001$, indicate a statistical difference with the control. $^{\#}P < .05$, $^{\#\#}P < .01$, and $^{\#\#\#}P < .001$, indicate a significant difference with the MMC-treated control.

and 293T-PGS shRNA cells compared with wild-type 293T (Figure 6 *E* and *F*).

The wild-type, CDS-2 shRNA-, and PGS shRNA-expressing stable clones were also established in p53-null H1299 cells. In H1299 models, both the Bcl-$2_{mitochondria/whole}$ and Bcl-$xL_{mitochondria/whole}$ ratios were strongly reduced in relation to the 293T models with saturated p53 expression. However, the Bcl-$2_{mitochondria/whole}$ and Bcl-$xL_{mitochondria/whole}$ ratios did not statistically differ among H1299 models (Figure 6, *E* and *F*). Interestingly, in both 293T and H1299 models, the decrease in Bcl-$xL_{mitochondria/whole}$ ratio was more obvious than that in the Bcl-$2_{mitochondria/whole}$ ratio, suggesting that the mitochondrial partition of Bcl-xL was more dependent on mitochondrial p53 translocation. The elevation of Bcl-$xL_{mitochondria/whole}$ ratio was found in H1299 models expressing pCEP4-p53wt ($P < .05$), suggesting that p53 acts as a carrier in the transportation of Bcl-xL to mitochondria directly. Moreover, the Bcl-$xL_{mitochondria/whole}$ ratio of H1299–CDS-2 shRNA was lower than H1299–wild-type and showed statistical significance.

Discussion

In past studies, the p53 was identified as a soluble nuclear protein. Three potential nuclear leading sequences (NLSs) and a leucine-rich nuclear export signal that are clustered in C-terminal region are required for p53 entry and retention in the nucleus [25]. Marchenko et al. [8] first demonstrated that death signals can induce p53 translocation to the mitochondria. In the present studies, we found that both membrane-bound p53 and the soluble form of p53 coexisted in the mitochondrial extract. The extraction discrepancies between bicarbonate and detergent might be due to an effect on the charge of p53, as well as the ionic effects. Moreover, a strong interaction between p53 and cardiolipin, a mitochondrion-restricted phospholipid, was also evidenced by an *in vitro* lipid-binding assay (Figure 2). Cardiolipin is strongly partitioned at contact sites and may interact with mitochondrial proteins through their positively charged signal sequences of precursor proteins [15,16]. Cytochrome *c* is one of the soluble basic proteins that resided in the mitochondrial inner membranes and was established to specifically bind to cardiolipin [26]. The binding of cytochrome *c* to cardiolipin results from electrostatic ion-ion interactions with positively charged lysine residues and negatively charged phosphate groups of cardiolipin or by a tightly hydrophobic interaction [21]. The peroxidation of cardiolipin disrupts binding and releases cytochrome *c* into the cytosol [26–28]. The nuclear homing domain usually consists of a basic amino acid core that may be the putative cardiolipin-binding region. Three potential NLSs are clustered at the C-terminal region of p53: NLS I (313-322, PPQKKKPLDG), NLS II (366-369, KTKK), and NLS III (375-380, SHRKKTM). All three NLSs are enriched in the positively charged lysine residues and are predicted to be an electrostatic center [29–31]. The prediction was demonstrated by the potential of different p53-GST fusion protein fragments to interact with cardiolipin. Compared with full-length p53, the p53 polypeptides 319-393 (with NLS II and III) and 101-318 (with a partial NLS I) showed 75% and 25% cardiolipin-binding abilities, respectively (Figure 2). These findings suggest that the C-terminal of p53 is the major region required for p53-cardiolipin interaction. Cardiolipin is a main component of the mitochondrial inner membrane. However, Marchenko et al. [8] previously reported that p53 predominantly localizes to the surface of the mitochondria. The apparent discrepancy may be explained by the electrostatic ion-ion interactions between p53 and other anionic phospholipids, including phosphatidylglycerol and phosphatidic acid. Both phosphatidylglycerol and phosphatidic acid are precursors of cardiolipin. Moreover, the interaction to phosphatidic acid was more convincing than that to cardiolipin, suggesting the involvement of p53 protein in earlier *de novo* cardiolipin biosynthesis pathway. The p53-phospholipids interaction might contribute to the p53's translocation to the mitochondria during cardiolipin biosynthesis.

The classic method of mitochondrial protein importation requires the mitochondrial leading signal peptides and the recognition of the Tom complex [32]. In a recent study, mutant p53 with an aberrant conformation was translocated to the mitochondria through protein-protein interactions with a chaperon system, such as hsp70 [13], hsp90, and cochaperones [14]. Translocation of p53 to the mitochondria through its binding to cardiolipin may be a potential mechanism. The Bid protein also showed cardiolipin-, phosphatidylglycerol-, and phosphatidic acid–binding activities. Bid-phospholipid interactions facilitate Bid translocation to the mitochondria and result in cytochrome *c* release

[33–35]. The mitochondrial translocation model of Bid and p53 through cardiolipin transfer activity provides an interesting and novel mitochondrial protein importation pathway. *De novo* cardiolipin biosynthesis occurs in three enzymatic steps, including CDS, PGS, and CLS. The CLS protein depletion might cause a lethal effect [36,37]. In the present studies, RNA interference by the PGS and CDS-2 shRNA constructs was used to suppress endogenous PGS and CDS-2 expressions. Disruption of cardiolipin biosynthesis diminished the content of mitochondrial p53 translocation (Figures 3 and 4). Our data revealed that cardiolipin and its precursors might function as a carrier and facilitate p53 transfer to mitochondria (Figure W3).

Aside from p53 mitochondrial translocation, a p53-dependent translocation of antiapoptotic Bcl-xL and Bcl-2 to the mitochondria has also been found [36–38]. A coimmunoprecipitation study showed that p53 and the Bcl-xL/Bcl-2 complex were colocalized [36]. On the basis of our study, the p53-dependent Bcl-xL and Bcl-2 mitochondrial translocation was also determined by their content in cytosolic pool. The changes of Bcl-xL and Bcl-2 level in the whole lysate resulted in increasing (low-dose MMC treatment) or decreasing (high-dose MMC treatment) mitochondrial translocation. In HEK 293T–CDS-2 shRNA cell, the mitochondrial distribution of Bcl-xL and Bcl-2 was reduced compared with wild type. Furthermore, Bcl-xL and Bcl-2 mitochondrial partition was strongly reduced in p53-null H1299 models and was rescued in H1299 models with pCEP4-p53wt expression (Figure 6). We thought the mitochondrial distribution of Bcl-xL and Bcl-2 is regulated by mitochondrial p53 translocation (Figure W3). Also, we found

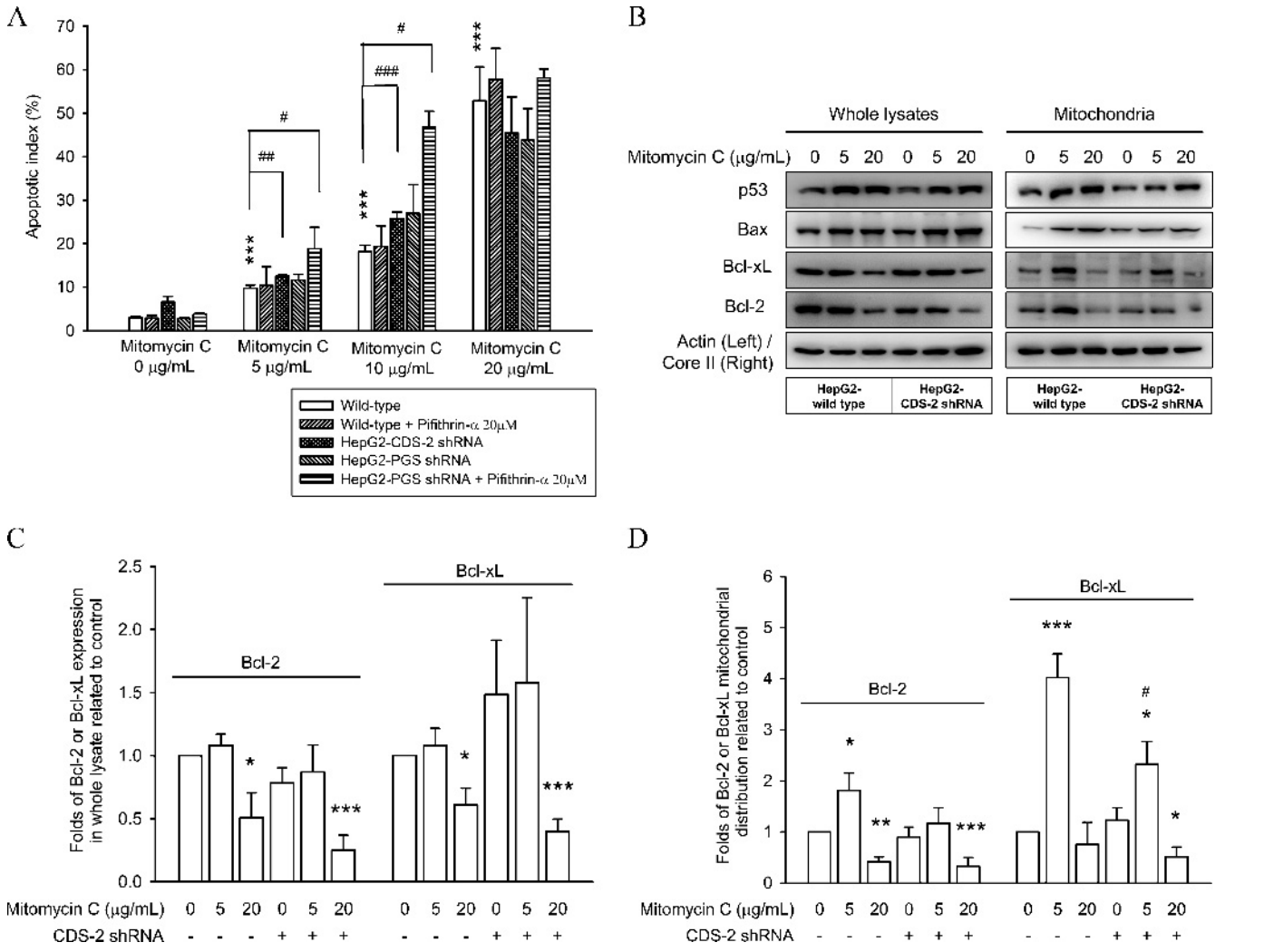

Figure 5. Decrease mitochondrial p53 content and p53-dependent Bcl-xL or Bcl-2 mitochondrial partition enhanced MMC-induced cell death. (A) Cells were prepared and treated with MMC for 24 hours. Pretreatment with 20 μM pifithrin-α was carried out for 30 minutes before MMC incubation. The apoptotic index was analyzed by propidium iodide staining and flow cytometry as described in Materials and Methods. $^{***}P < .001$, indicates a statistical difference with the control. $^{\#}P < .05$, $^{\#\#}P < .01$, and $^{\#\#\#}P < .001$, indicate a statistical difference with MMC-treated groups. (B) The expression of p53, Bax, Bcl-xL, and Bcl-2 and their mitochondrial distributions were analyzed in MMC-treated HepG2–wild-type and HepG2–CDS-2 shRNA cells. Both cell types were incubated with 5 and 20 μg/ml MMC for 6 hours. Low-dose (5 μg/ml) MMC treatment did not change Bcl-xL and Bcl-2 protein expressions in either HepG2–wild-type or HepG2–CDS-2 shRNA cells. However, as a limitation of mitochondrial p53 translocation, 5 μg/ml MMC treatment decreased Bcl-xL and Bcl-2 mitochondrial distributions in HepG2–CDS-2 shRNA cells. High-dose (20 μg/ml) MMC treatment strongly decreased Bcl-xL and Bcl-2 protein expressions in both HepG2–wild-type and HepG2–CDS-2 shRNA cells, resulting in the decrease in their mitochondrial distribution. (C and D) The Bcl-xL and Bcl-2 expression level in whole lysate (C) and their mitochondrial distributions (D) were analyzed by densitometry. $^{*}P < .05$, $^{**}P < .01$, $^{***}P < .001$, indicate a statistical difference with the control. $^{\#}P < .05$, indicates a statistical difference with MMC-treated groups.

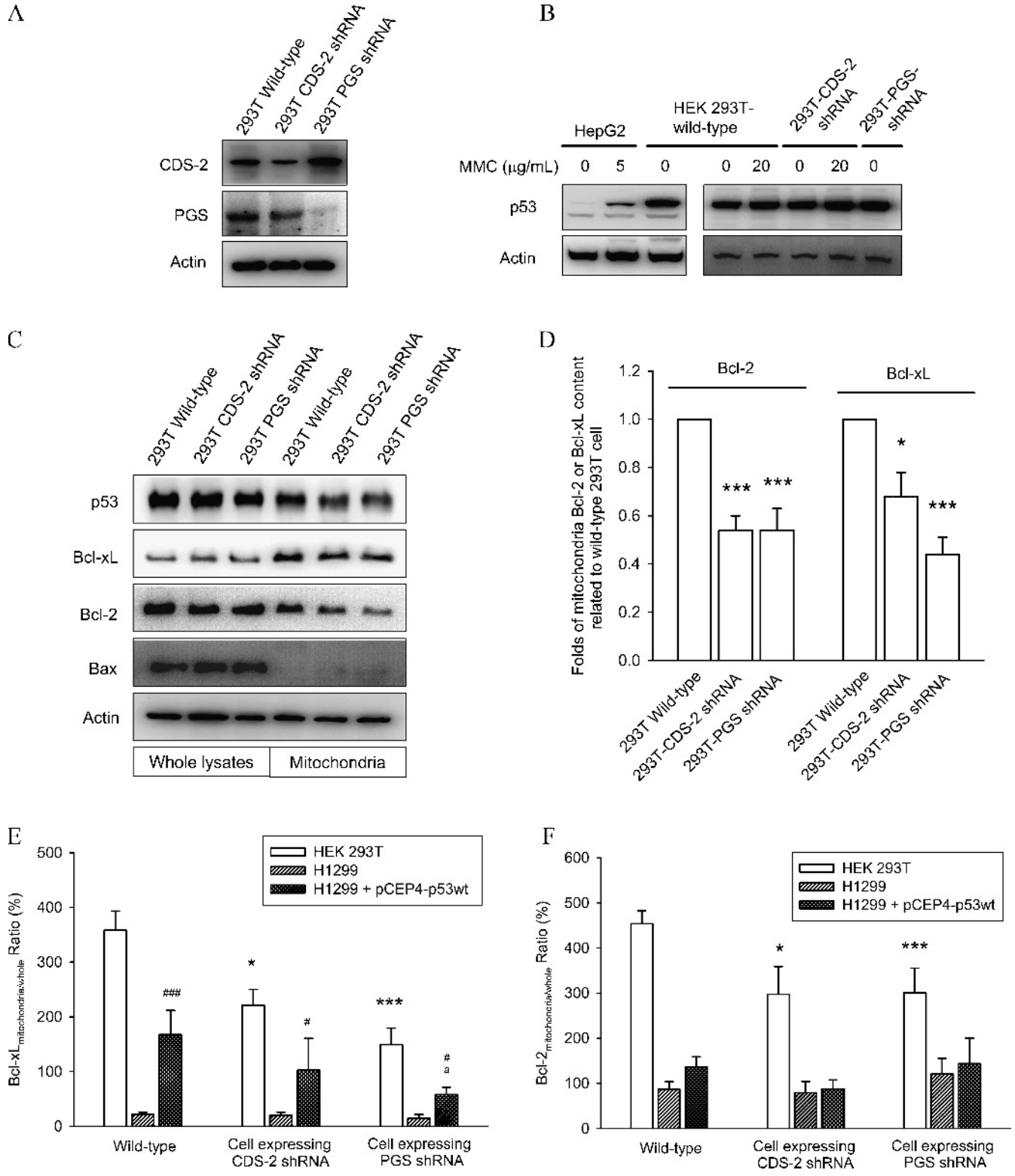

Figure 6. The expression and mitochondrial distribution of Bcl family members in HEK 293T cell stable clones expressing CDS-2 shRNA and PGS shRNA. (A) The CDS-2 shRNA- and PGS shRNA-expressing stable clone was selected in HEK 293T cells. (B) HEK 293T models have a higher p53 protein basal level. With the addition of 20 μg/ml MMC, the p53 protein content was not upregulated in 293T–wild-type, 293T–CDS-2 shRNA, and 293T-PGS shRNA cells, suggesting that the p53 status was saturated in the HEK 293T models. (C) The mitochondrial distributions of p53, Bcl-2, and Bcl-xL were analyzed in 293T cell models. The mitochondrial distribution of Bcl-2 and Bcl-xL was reduced in 293T–CDS-2 shRNA and 293T-PGS shRNA cells in relation to wild-type 293T cell. (D) The Bcl-2 and Bcl-xL mitochondrial translocations were analyzed by densitometry. The $\text{Bcl-2}_{\text{mitochondria/whole}}$ ratio (E) and $\text{Bcl-xL}_{\text{mitochondria/whole}}$ ratio (F) were calculated from three HEK 293T cell models and p53-null H1299 cell models and indicate a statistical difference in relation to the wild-type control. $^{*}P < .05$ and $^{***}P < .001$, indicate a statistical difference between HEK 293T models. $^{\#}P < .05$ and $^{\#\#\#}P < .001$, indicate a statistical difference between H1299 models. $^{a}P < .05$, indicates a statistical difference between H1299–wild-type control with pCEP4-p53wt expression.

that the change in the p53-dependent Bcl-xL mitochondrial translocation was more evident than that in the Bcl-2. It has been demonstrated that p53 could interact with Bcl-xL directly not only by mapping binding domain analysis but also by the space-filling model [10]. It may be the reason that Bcl-xL mitochondrial partition was blocked completely in p53-null H1299 models (compared with HEK 293T models with saturated p53). Because the evidence for a p53/Bcl-2 interaction was deficient, the p53-dependent Bcl-2 mitochondrial translocation may be an indirect response (Bcl-xL/Bcl-2 interaction first, followed by p53 interaction with Bcl-xL). This reason can also explain why the Bcl-2 mitochondrial partition is lower than that of the Bcl-xL when p53 protein was introduced into the p53-null H1299 models.

In the nucleus, p53 functions as a transcription factor through the DNA-binding domain (102-292) but also represses gene expression through an interaction with histone deacetylases [39]. The p53-dependent transcription of proapoptotic products, such as Bax [5], p53-inducible genes [4,7], BH3-only proteins Noxa [40], PUMA [41], and $p53^{AIP1}$ [42], can directly or indirectly disrupt mitochondrial integrity and cause cytochrome *c* release. In another pathway, the p53 protein is translocated to the mitochondria and physically interacts with Bcl-xL [10,11], Bak [43], or manganese superoxide dismutase [12] in the mitochondria. The *in vivo* significance and potential consequences of these interactions were determined at the onset of p53-dependent apoptosis preceding changes in redox balance, mitochondrial membrane potential, cytochrome *c* release, and caspase activation [8,12]. Emerging publications suggest that after genetic stress, a fraction of p53 translocates into the mitochondria, inducing cytochrome *c* release and apoptosis [8,37,44–47]. However, based on our study, we thought mitochondrial p53 may regulate apoptosis in a "biphasic" manner. It means that under the low-dose MMC treatment, the increase in p53 and p53-dependent Bcl-xL (and Bcl-2) mitochondrial translocation might attenuate apoptosis progression. The prediction was proved in MMC-induced apoptotic index among HepG2 models. In CDS-2 shRNA- and PGS shRNA-expressing cells, the content of mitochondrial p53, Bcl-2, and Bcl-xL decreased, and the apoptotic cell population was enhanced. We did found the cytochrome *c* release and caspase-3 activation in MMC-treated cells in a dose-dependent manner, but no statistical significance was found in either the amounts of cytochrome *c* release or the activation of caspase-3 between HepG2–wild-type and HepG2–CDS-2 shRNA cells (data not shown). These data suggest that mitochondrial p53 and p53-dependent Bcl-xL (and Bcl-2) mitochondrial distribution possess unfound functions in regulating apoptotic progression. It is important to note the mitochondrial localization of the p53 protein in proliferative cells [48]. Mitochondrial p53 localization in normal conditions agrees with the recent observation of a direct positive influence of p53 on mitochondrial biogenesis and aerobic metabolism [49]. Mitochondrial p53 also exerts physical interactions with mitochondria DNA and DNA polymerase γ and enhances error correction activities [50]. However, the documentation of apoptotic enhancement is without statistical difference in the high-dose MMC treatment. In the high-dose condition, the mitochondrial p53 represents a pool of p53 at the outer membrane, thus after induction of apoptosis, p53 induces outer membrane permeability and apoptosis.

In a *Saccharomyces cerevisiae* model, disruption of CLS (*CRD1*) caused mitochondrial anion phospholipids depletion [20,51], mitochondrial electron transport repression [19], and apoptosis [52]. It means that the apoptotic enhancement in our study may be because cardiolipin is required for normal mitochondrial apoptotic regulation. To address this issue, the mitochondrial functions, including cellular ATP level, mitochondrial membrane potential, and cell proliferation capacity, were evaluated in PGS shRNA- and CDS-2 shRNA-expressing cells. Neither ATP biosynthesis nor mitochondrial membrane potential was changed in these cells (Figure W2), suggesting that the mitochondrial functions remained unaffected by the transfection of CDS-2 shRNA and PGS shRNA. Also, the proliferation capacities were without changes in these cells. In MMC-treated HepG2-PGS shRNA cell, the pretreatment of pifithrin-α inhibited mitochondrial p53 translocation and resulted in apoptosis enhancement. However, neither mitochondrial p53 translocation nor apoptosis enhancement was found in the same treatment but without pifithrin-α pretreatment (Figure 5*A*). Hence, the finding of this study resulted from mitochondrial p53 content and p53-dependent Bcl member mitochondrial distribution.

In the present study, we first found an electrostatic ion-ion interaction among p53 protein and cardiolipin, phosphatidylglycerol, and phosphatidic acid. Disruption of cardiolipin biosynthesis by PGS shRNA or CDS-2 shRNA transfection eliminated MMC-induced mitochondrial p53 translocation, suggesting the crucial role of cardiolipin in the translocation of p53 to the mitochondria. Disruption of cardiolipin biosynthesis also limited the translocation of Bcl-xL and Bcl-2 to the mitochondria and sensitized cells in response to mild genotoxic stimulation (Figure W3).

References

[1] Vogelstein B, Land D, and Levine AJ (2000). Surfing the p53 network. *Nature* **408**, 307–310.

[2] Vousden KH (2000). p53: death star. *Cell* **103**, 691–694.

[3] Woods DB and Vousden KH (2001). Regulation of p53 function. *Exp Cell Res* **264**, 56–66.

[4] Takeshi T, Ken M, Rishu T, Minoru T, Koichi T, Tsuzuku M, Shinya M, Takuya M, Tetsuji T, Junji K, et al. (2003). Induction of PIG3 and NOXA through acetylation of p53 at 320 and 373 lysine residues as a mechanism for apoptotic cell death by histone deacetylase inhibitors. *Cancer Res* **63**, 8948–8954.

[5] Chipuk JE, Kuwana T, Bouchier-Hayes L, Droin NM, Newmeyer DD, Schuler M, and Green DR (2004). Direct activation of bax by p53 mediates mitochondrial membrane permeabilization and apoptosis. *Science* **303**, 1010–1014.

[6] Matoba S, Kang JG, Patino WD, Wragg A, Boehm M, Gavrilova O, Hurley PJ, Bunz F, and Hwang PM (2006). p53 regulates mitochondrial respiration. *Science* **312**, 1650–1653.

[7] Donald SP, Sun XY, Hu CA, Yu J, Mei JM, Valle D, and Phang JM (2001). Proline oxidase, encoded by p53-induced gene-6, catalyzes the generation proline-dependent reactive oxygen species. *Cancer Res* **61**, 1810–1815.

[8] Marchenko ND, Zaika A, and Moll UM (2000). Death signal–induced localization of p53 protein to mitochondria. *J Biol Chem* **275**, 16202–16212.

[9] Erster S, Mihara M, Kim RH, Petrenko O, and Moll UM (2004). Mitochondrial p53 translocation triggers a rapid first wave of cell death in response to DNA damage that can precede p53 target gene activation. *Mol Cell Biol* **24**, 6728–6741.

[10] Mihara M, Erster S, Zaika A, Petrenko O, Chittenden T, Pancoska P, and Moll UM (2003). P53 has a direct apoptogenic role at the mitochondria. *Mol Cell* **11**, 577–590.

[11] Park BS, Song YS, Yee SB, Lee BG, Seo SY, Park YC, Kim JM, Kim HM, and Yoo YH (2005). Phospho–Ser 15–p53 translocates into mitochondria and interacts with Bcl-2 and Bcl-xL in eugenol-induced apoptosis. *Apoptosis* **10**, 193–200.

[12] Zhao Y, Chaiswing L, Velez JM, Batinic-Haberle I, Colburn NH, Oberley TD, and Clair DK (2005). p53 translocation to mitochondria precedes its nuclear translocation and targets mitochondrial oxidative defense protein-manganese superoxide dismutase. *Cancer Res* **65**, 3745–3750.

[13] King FW, Wawrzynow A, Hohfeld J, and Zylicz M (2001). Co-chaperones Bag-1, Hop and Hsp40 regulate Hsc70 and Hsp90 interactions with wild-type or mutant p53. *EMBO J* **20**, 6297–6305.

[14] Merrick BA, He C, Witcher LL, Patterson RM, Reid JJ, Pence-Pawlowski PM, and Selkirk JK (1996). HSP binding and mitochondrial localization of p53 protein in human HT1080 and mouse C3H10T1/2 cell lines. *Biochim Biophys Acta* **1297**, 57–68.

[15] Daum G and Vance JE (1997). Import of lipids into mitochondria. *Prog Lipid Res* **36**, 103–130.

[16] Ardail D, Privat JP, Egret-Charlier M, Levrat C, Lerme F, and Louisot P (1990). Mitochondrial contact sites. Lipid composition and dynamics. *J Biol Chem* **265**, 18797–18802.

[17] Schlame M, Rua D, and Greenberg ML (2000). The biosynthesis and functional role of cardiolipin. *Prog Lipid Res* **39**, 257–288.

[18] Lu B, Xu FY, Jiang YJ, Choy PC, Hatch GM, Grunfeld C, and Feingold KR (2006). Cloning and characterization of a cDNA encoding human cardiolipin synthase (hCLS1). *J Lipid Res* **47**, 1140–1145.

[19] Ostrander DB, Zhang M, Mileykovskaya E, Rho M, and Dowhan W (2001). Lack of mitochondrial anionic phospholipids causes an inhibition of translation of protein components of the electron transport chain. A yeast genetic model system for the study of anionic phospholipid function in mitochondria. *J Biol Chem* **276**, 25262–25272.

[20] Feng J, Ryan MT, Schlamei M, Zhao M, Gu Z, Klingenberg M, Pfanner N, and Greenberg ML (2000). Absence of cardiolipin in the crd1 null mutant results in decreased mitochondrial membrane potential and reduced mitochondrial function. *J Biol Chem* **275**, 22387–22394.

[21] Piccotti L, Marchetti C, Migliorati G, Roberti R, and Corazzi L (2002). Exogenous phospholipids specifically affect transmembrane potential of brain mitochondria and cytochrome *c* release. *J Biol Chem* **277**, 12075–12081.

[22] Eskes R, Desagher S, Antonsson B, and Martinou JC (2000). Bid induces the oligomerization and insertion of Bax into the outer mitochondrial membrane. *Mol Cell Biol* **20**, 929–935.

[23] Smith DB and Johnson KS (1988). Single-step purification of polypetides expressed in *Escherichia coli* as fusions with glutathione *S*-transferase. *Gene* **67**, 31–40.

[24] Li CH, Tzeng SL, Cheng YW, and Kang JJ (2005). Chloramphenicol-induced mitochondrial stress increases p21 expression and prevents cell apoptosis through a p21-dependent pathway. *J Biol Chem* **280**, 26193–26199.

[25] Volta M, Bulfone A, Gattuso C, Rossi E, Mariani M, Consalez GG, Zuffardi O, Ballabio A, Banfi S, and Franco B (1999). Identification and characterization of CDS2, a mammalian homolog of the *Drosophila* CDP-diacylglycerol synthase gene. *Genomics* **55**, 68–77.

[26] Ott M, Robertson JD, and Gogvadze V (2002). Cytochrome *c* release from mitochondria proceeds by a two-step process. *Proc Natl Acad Sci USA* **99**, 1259–1263.

[27] Nomura K, Imai H, and Koumura T (2000). Mitochondrial phospholipid hydroperoxide glutathione peroxidase inhibits the release of cytochrome *c* from mitochondria by suppressing the peroxidation of cardiolipin in hypoglycaemia-induced apoptosis. *Biochem J* **351**, 183–193.

[28] Shidoji Y, Hayashi K, and Komura S (1999). Loss of molecular interaction between cytochrome *c* and cardiolipin due to lipid peroxidation. *Biochem Biophys Res Commun* **264**, 343–347.

[29] Stommel JM, Marchenko ND, Jimenez GS, Moll UM, Hope TJ, and Wahl GM (1999). A leucine-rich nuclear export signal in the p53 tetramerization domain: regulation of subcellular localization and p53 activity by NES masking. *EMBO J* **18**, 1660–1672.

[30] Schlattner U, Gehring F, Vernoux N, Tokarska-Schlattner M, Neumann D, Marcillat O, Vial C, and Wallimann T (2004). C-terminal lysines determine phospholipid interaction of sarcomeric mitochondrial creatine kinase. *J Biol Chem* **279**, 24334–24342.

[31] Shaulsky G, Goldfinger N, Ben-Zeev A, and Rotter V (1990). Nuclear accumulation of p53 protein is mediated by several nuclear localization signals and plays a role in tumorigenesis. *Mol Cell Biol* **10**, 6565–6577.

[32] Hood DA and Joseph AM (2004). Mitochondrial assembly: protein import. *Proc Nutr Soc* **63**, 293–300.

[33] Esposti MD, Erler JT, Hickman JA, and Dive C (2002). Bid, a widely expressed proapoptotic protein of the Bcl-2 family, displays lipid transfer activity. *Mol Cell Biol* **21**, 7268–7276.

[34] Lutter M, Fang M, Luo X, Nishijima M, Xie X, and Wang X (2000). Cardiolipin provides specificity for targeting of tBid to mitochondria. *Nat Cell Biol* **2**, 754–761.

[35] Gonzalvez F, Bessoule JJ, Rocchiccioli F, Manon S, and Petit PX (2005). Role of cardiolipin on tBid and tBid/Bax synergistic effects on yeast mitochondria. *Cell Death Differ* **12**, 659–667.

[36] Bivik CA, Larsson PK, Kagedal KM, Rosdahl IK, and Ollinger KM (2006). UVA/B induced apoptosis in human melanocytes involves translocation of cathepsins and Bcl-2 family members. *J Invest Dermatol* **126**, 1119–1127.

[37] Waster PK and Mollinger K (2009). Redox-dependent translocation of p53 to mitochondria or nucleus in human melanocytes after UVA- and UVB-induced apoptosis. *J Invest Dermatol* **129**, 1769–1781.

[38] Endo H, Kamada H, Nito C, Nishi T, and Chan PH (2006). Mitochondrial translocation of p53 mediates release of cytochrome *c* and hippocampal CA1 neuronal death after transient global cerebral ischemia in rats. *J Neurosci* **26**, 7974–7983.

[39] Murphy M, Ahn J, Walker KK, Hoffman WH, Evans RM, Levine AJ, and George DL (1999). Transcriptional repression by wild-type p53 utilizes histone deacetylases, mediated by interaction with mSin3a. *Genes Dev* **13**, 2490–2501.

[40] Oda E, Ohki R, Murasawa H, Nemoto J, Shibue T, Yamashita T, Tokino T, Taniguchi T, and Tanaka N (2000). Noxa, a BH3-only member of the Bcl-2 family and candidate mediator of p53-induced apoptosis. *Science* **288**, 1053–1058.

[41] Biswas SC, Ryu E, Park C, Malagelada C, and Greene LA (2005). Puma and p53 play required roles in death evoked in a cellular model of Parkinson disease. *Neurochem Res* **30**, 839–845.

[42] Matsuda K, Yoshida K, Taya Y, Nakamura K, Nakamura Y, and Arakawa H (2002). $p53^{AIP1}$ regulates the mitochondrial apoptotic pathway. *Cancer Res* **62**, 2883–2889.

[43] Leu JI, Dumont P, Hafey M, Murphy ME, and George DL (2004). Mitochondrial p53 activates Bak and causes disruption of a Bak-Mcl1 complex. *Nat Cell Biol* **6**, 443–450.

[44] Nemajerova A, Wolff S, Petrenko O, and Moll UM (2005). Viral and cellular oncogenes induce rapid mitochondrial translocation of p53 in primary epithelial and endothelial cells early in apoptosis. *FEBS Lett* **579**, 6079–6083.

[45] Skankar S and Srivastava RK (2007). Involvement of Bcl-2 family members, phosphatidylinositol 3′-kinase/AKT and mitochondrial p53 in curcumin (diferulolylmethane)-induced apoptosis in prostate cancer. *Int J Oncol* **30**, 905–918.

[46] Heyne K, Schmitt K, Mueller D, Armbruester V, Mestres P, and Roemer K (2008). Resistance of mitochondrial p53 to dominant inhibition. *Mol Cancer* **7**, 54.

[47] Vaseva AV, Marchenko ND, and Moll UM (2009). The transcription-independent mitochondrial p53 program is a major contributor to nutlin-induced apoptosis in tumor cells. *Cell Cycle* **11**, 1711–1719.

[48] Ferecatu I, Bergeaud M, Rodríguez-Enfedaque A, Le Floch N, Oliver L, Rincheval V, Renaud F, Vallette FM, Mignotte B, and Vayssière JL (2009). Mitochondrial localization of the low level p53 protein in proliferative cells. *Biochem Biophys Res Commun* **387**, 772–777.

[49] Saleem A, Adhihetty PJ, and Hood DA (2009). Role of p53 in mitochondrial biogenesis and apoptosis in skeletal muscle. *Physiol Genom* **37**, 58–66.

[50] Bakhanashvili M, Grinberg S, Bondal E, Simon AJ, Moshitch-Moshkovitz S, and Rahav G (2008). p53 in mitochondria enhances the accuracy of DNA synthesis. *Cell Death Differ* **15**, 1865–1874.

[51] Tuller G, Hrastnik C, Achleitner G, Schiefthaler U, Klein F, and Daum G (1998). YDL142c encodes cardiolipin synthase (Cls1p) and is non-essential for aerobic growth of *Saccharomyces cerevisiae*. *FEBS Lett* **421**, 15–18.

[52] Choi SY, Gonzalvez F, Jenkins GM, Slomianny C, Chretien D, Arnoult D, Petit PX, and Frohman MA (2007). Cardiolipin deficiency releases cytochrome *c* from the inner mitochondrial membrane and accelerates stimuli-elicited apoptosis. *Cell Death Differ* **14**, 597–606.

Supplementary Data

Supplementary Methods

MTT assay. Cells were seeded in 6-well (transiently transfected HepG2) or 48-well (HEK 293T and H1299 stable clones with the density of 1×10^4 cells per well) plates. For HepG2 transfection, the shRNA (1-5 μg per well) was transfected by using PolyJet *in vitro* DNA transfection reagent (SignaGen Laboratory) for 24 hours as described in Materials and Methods. For HEK 293T and H1299 cell proliferation assay, the cell densities were determined by MTT assay after 24 to 48 hours of incubation. Before MTT assay, the 3-(4,5-dimethyl-2-thiazolyl)-2,5-diphenyl-2*H*-tetrazolium bromide (MTT) was added to each well to achieve a final concentration of 0.04 mg/ml. After 4 hours of incubation, the MTT solution was removed and replaced with 200 μl of DMSO. Absorbance of the MTT metabolic product, formazan, at 570 nm was measured with an ELISA reader. Reading was corrected for the background optical density by subtracting the readings from a blank treatment.

Cytosolic ATP content determination. Total cellular ATP level was determined by bioluminescence using an ATP-bioluminescent assay kit (BioVision, Mountain View, CA). Cells were lysed in lysis buffer and centrifuged (12,000*g* for 5 minutes). Each reaction was performed by mixing 5 to 10 μl of supernatant in 90 μl of reaction buffer in a 96-well plate. Finally, luciferase and luciferase substrates were added, and luminescence intensity was counted immediately using a luminometer (Berthord, Oak Ridge, TN) calibrated with the appropriate ATP standards.

Mitochondrial membrane potential measurement. Cells were seeded in six-well plates. Twenty-four hours after seeding, 40 nM $DiOC_6$ was added and incubated for 30 minutes at 37°C. $DiOC_6$ is a lipophilic fluorochrome enriched in positive charge that diffuses across the inner membrane dependent on mitochondrial membrane potential. Finally, cells were harvested by trypsinization and washed two to three times by PBS. The fluorescent intensity was measured by flow cytometry with the FL-1 filter (BD Biosciences, San Jose, CA).

Cardiolipin level determination. Cellular cardiolipin level was determined by its specific fluorescent probe, 10-*N*-nonyl acridine orange (NAO), and evaluated by flow cytometry or fluorescent microscopy. Cells were harvested by trypsinization and fixed in 4% paraformaldehyde for 10 to 15 minutes. Cell density was adjusted to 1×10^5 cells/ml and stained with 10 μM NAO for 30 minutes at room temperature. Stained cells were then washed twice with PBS. The NAO fluorescent intensity was measured by flow cytometry. For fluorescent microscopy, H1299 stable clones were seeded on cover glass. Cells were fixed in 4% paraformaldehyde followed by NAO staining for 30 minutes. Stained cells were then washed twice with PBS. After mounting, cells were observed under a Leica fluorescent microscope.

Results

PGS shRNA and CDS-2 shRNA knockdown effects were determined by cellular cardiolipin level. The fluorescent probe NAO that could specifically bind to cardiolipin has been demonstrated. The NAO-stained HepG2, HEK 293T, and H1299 cells were analyzed by fluorescent microscopy or flow cytometry. The NAO fluorescent intensity decreased approximately by 15% to 20% (transiently transfected HepG2 models) and 40% to 50% (HEK 293T stable clone models) compared with their wild-type cells (Figure W1, *A* and *B*). In H1299 stable clones, the NAO fluorescent intensity also decreased in PGS shRNA-transfected H1299 cell (H1299-PGS shRNA) and H1299–CDS-2 shRNA (compared with H1299–wild-type cell; Figure W1*C*). These data suggested that the PGS shRNA and CDS-2 shRNA do work and decrease cardiolipin biosynthesis.

Evaluation of mitochondria function of HepG2, HEK 293T, and H1299 models expressing PGS shRNA or CDS-2 shRNA. Cardiolipin depletion may alter mitochondria function. Hence, the outcome of this study might result from mitochondrial function changes rather than p53 translocation. To address this issue, the mitochondrial functions, including cellular ATP level and mitochondrial membrane potential, were evaluated in CDS-2 shRNA-expressing cell. In ATP biosynthesis, the cellular ATP contents were without significant differences among wild-type, PGS shRNA-, and CDS-2 shRNA-expressing cells (both transiently transfected HepG2 and HEK 293T stable clones) (Figure W2*A*). The mitochondrial membrane potentials were also without significant differences among wild-type, PGS shRNA-, and CDS-2 shRNA-expressing cells (Figure W2*B*). Moreover, mitochondrial damages often decrease cell proliferation. In HepG2, the transient transfection of PGS shRNA and CDS shRNA did not cause the decrease in cell densities. In both HEK 293T and H1299 models, their proliferation was without statistical differences among wild-type, CDS-2 shRNA-, and PGS shRNA-expressing cells (Figure W2*C*). These data proved that the mitochondrial functions remained unaffected by the transfection of CDS-2 shRNA and PGS shRNA. Hence, the finding of this study has high relation to the mitochondrial p53 content.

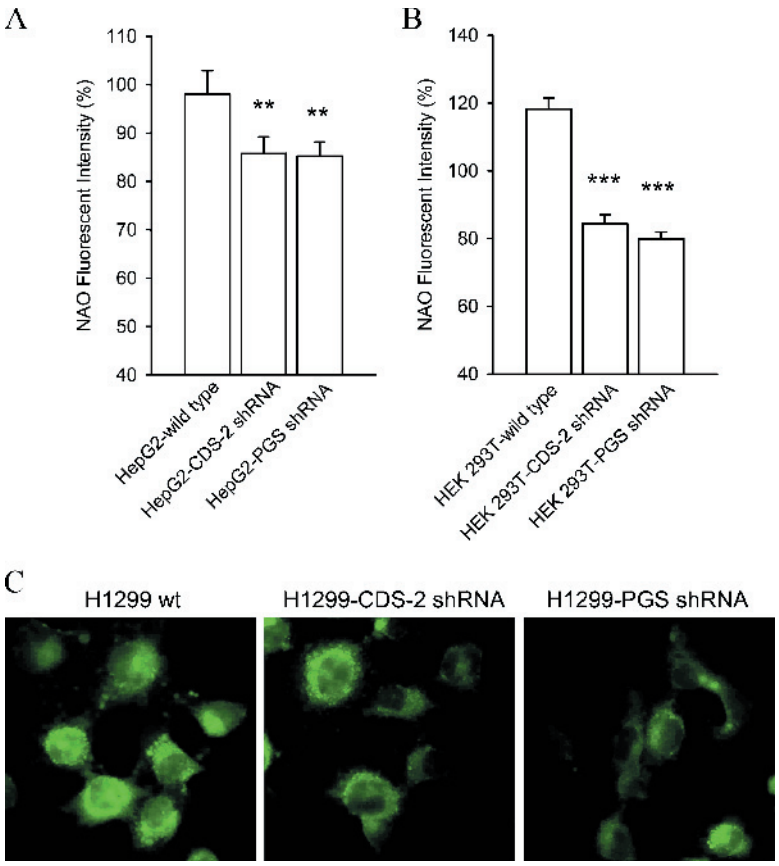

Figure W1. Detection of cardiolipin levels in HepG2, HEK 293T, and H1299 models by NAO staining. (A) HepG2 was transfected transiently with CDS-2 shRNA or PGS shRNA for 24 hours by using PolyJet *in vitro* DNA transfection reagent (SignaGen Laboratory) as described in Materials and Methods. (B and C) The HEK 293T and H1299 stable clones were selected by puromycin as described in Materials and Methods. In HepG2, HEK 293T, and H1299 models, the fluorescent intensity decreased in PGS shRNA- and CDS-2 shRNA-expressing cells compared with wild-type control. $^{**}P < .05$, $^{***}P < .001$, indicate a statistical difference with the control.

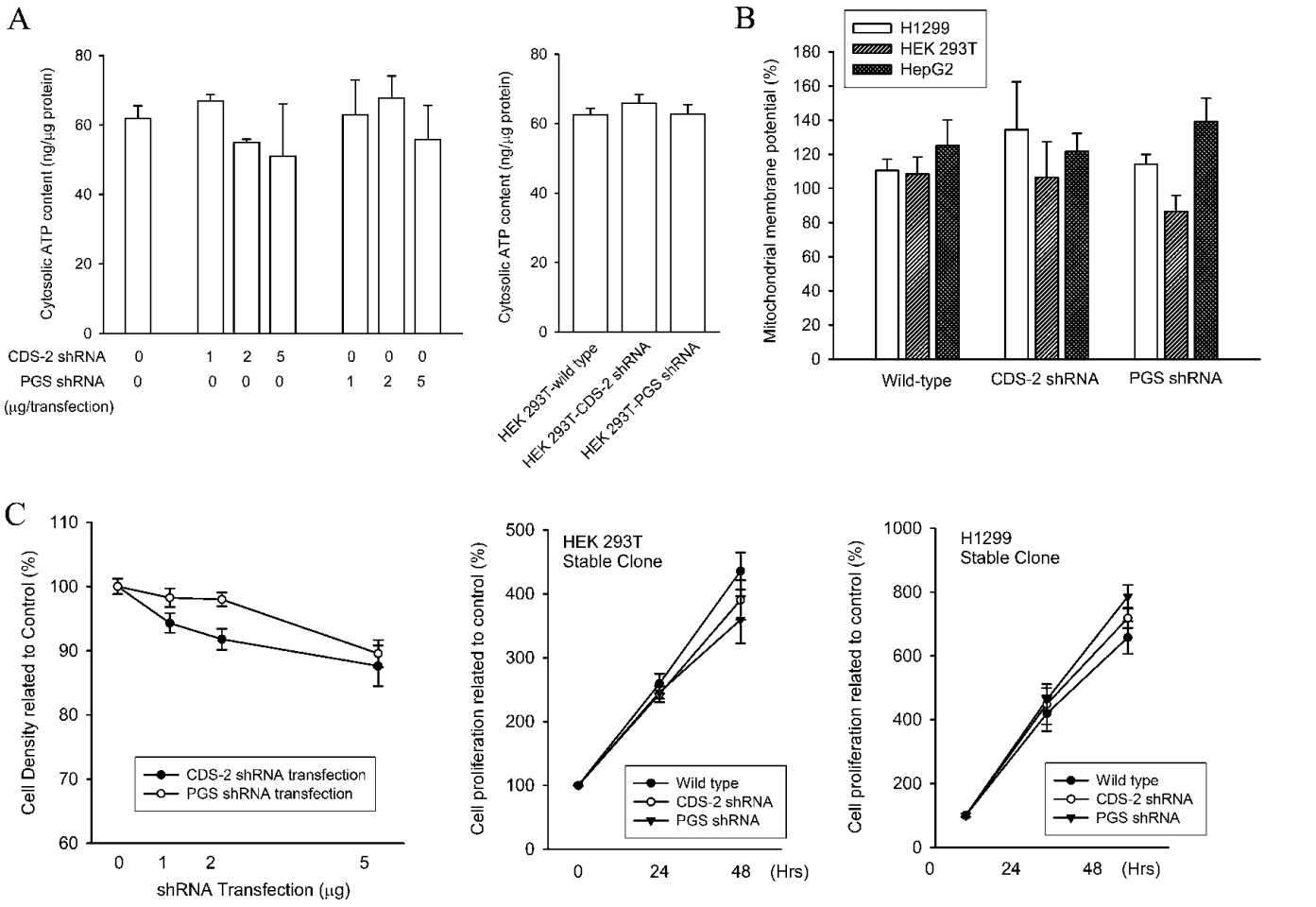

Figure W2. Evaluation of mitochondria function of HepG2, HEK 293T, and H1299 models expressing PGS shRNA or CDS-2 shRNA. (A) Cellular ATP level was determined as described in Supplementary Methods. In transiently transfected HepG2 and HEK 293T stable clones, the cellular ATP contents were without significant differences among wild-type, PGS shRNA-, and CDS-2 shRNA-expressing cells. (B) Mitochondrial membrane potential was determined by $DiOC_6$ as described in Supplementary Methods. The mitochondrial membrane potentials were without significant differences among wild-type, PGS shRNA-, and CDS-2 shRNA-expressing cells. (C) Cell density and proliferation were determined by MTT assay as described in Supplementary Methods. In HepG2, the transient transfection of PGS shRNA or CDS-shRNA did not cause the decrease in cell density. In HEK 293T and H1299 stable clones, the proliferation capacities were without statistical differences among wild-type, CDS-2 shRNA-, and PGS shRNA-expressing cells.

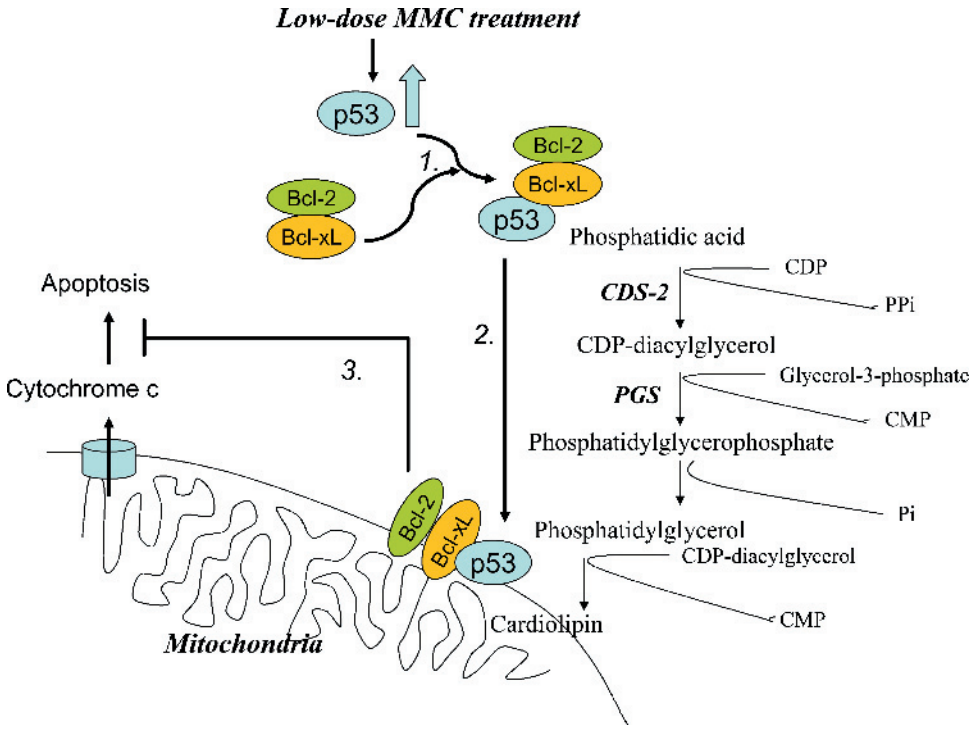

Figure W3. The perspective of p53 mitochondrial translocation and p53-dependent Bcl-xL mitochondrial translocation. 1. In the low-dose MMC treatment, the activated p53 accumulated in the cytosol, whereas the expression of Bcl-xL and Bcl-2 remained unaffected. The accumulated p53 interacted with Bcl-xL or Bcl-xL/Bcl-2 complex. However, in the high-dose MMC treatment, the expression of Bcl-xL and Bcl-2 decreased obviously and reduced their interaction with p53. 2. The p53 interacted with phosphatidic acid and anionic phospholipids in cardiolipin biosynthesis pathway, after which it translocated to mitochondria by its lipid transfer ability. Diminishing cardiolipin biosynthesis pathway by PGS shRNA and CDS-2 shRNA could eliminate p53 and p53-dependent Bcl-xL and Bcl-2 mitochondrial translocation. 3. In the low-dose MMC treatment, the p53-dependent Bcl-xL and Bcl-2 could attenuate cell death progression. However, in the high-dose MMC treatment, only the p53 protein translocated to mitochondria. The p53 at the outer membrane could induce outer membrane permeability and promote apoptosis.